Magnetopause erosion during the March 17, 2015, magnetic storm: Combined field-aligned currents, auroral oval, and magnetopause observations

G. Le[1], H. Lühr[2], B. J. Anderson[3], R. J. Strangeway[4], C. T. Russell[4], H. Singer[5], J. A. Slavin[6], Y. Zhang[3], T. Huang[2], K. Bromund[1], P. J. Chi[4], G. Lu[7], D. Fischer[8], E. L. Kepko[1], H. K. Leinweber[4], W. Magnes[8], R. Nakamura[8], F. Plaschke[8], J. Park[2], J. Rauberg[2], C. Stolle[2], and R. B. Torbert[9]

1. NASA Goddard Space Flight Center, Greenbelt, MD, USA
2. GFZ German Research Centre for Geosciences, Potsdam, Germany
3. The Johns Hopkins University Applied Physics Laboratory, Laurel, MD, USA
4. University of California, Los Angeles, CA, USA
5. NOAA Space Weather Prediction Center, Boulder, CO, USA
6. University of Michigan, Ann Arbor, MI, USA
7. High Altitude Observatory, UCAR, Boulder, CO, USA
8. Space Research Institute, Austrian Academy of Sciences, Graz, Austria
9. University of New Hampshire, Durham, NH, USA

GRL Paper #2016GL068257

Correspondence to:
Guan Le, Code 674, Space Weather Laboratory, NASA Goddard Space Flight Center, Greenbelt, MD 20771 (Guan.Le@nasa.gov)

Revision 3/9/2016

Abstract

We present multi-mission observations of field-aligned currents, auroral oval, and magnetopause crossings during the March 17, 2015 magnetic storm. Dayside reconnection is expected to transport magnetic flux, strengthen field-aligned currents, lead to polar cap expansion and magnetopause erosion. Our multi-mission observations assemble evidence for all these manifestations. After a prolonged period of strongly southward interplanetary magnetic field, Swarm and AMPERE observe significant intensification of field-aligned currents. The dayside auroral oval, as seen by DMSP, appears as a thin arc associated with ongoing dayside reconnection. Both the field-aligned currents and the auroral arc move equatorward reaching as low as ~60° MLat. Strong magnetopause erosion is evident in the in-situ measurements of the magnetopause crossings by GOES-13/15 and MMS. The coordinated Swarm, AMPERE, DMSP, MMS and GOES observations, with both global and in-situ coverage of the key regions, provide a clear demonstration of the effects of dayside reconnection on the entire magnetosphere.

Key Points:

- Observed manifestations of dayside reconnection on field-aligned currents and auroral oval
- Observed strong magnetopause erosion during storm main phase
- Demonstrated effects of dayside reconnection on entire magnetosphere

1. Introduction

Magnetopause erosion refers to earthward motion of the dayside magnetopause under southward interplanetary magnetic field (IMF) [Aubry et al., 1970]. The magnetopause is closer to Earth under southward IMF than under northward IMF for the same solar wind dynamic pressure and this erosion is attributed to the effects of dayside magnetic reconnection. The merging between the IMF and Earth's magnetic field creates open field lines that are transported tailward by the magnetosheath flow [Dungey, 1961]. In this process, magnetic flux is removed from the dayside and added into the tail lobe. The open flux is then closed by subsequent reconnection in the magnetotail and returned to the dayside by sunward convection. When the dayside reconnection rate exceeds the nightside rate, net flux is added to the nightside and the dayside magnetopause moves earthward. Signatures of magnetopause erosion are consistently observed in statistical studies of magnetopause location [Holzer and Slavin, 1978, 1979; Sibeck et al, 1991; Petrinec and Russell, 1996; Shue et al., 1997, 1998], statistical surveys of magnetospheric magnetic fields [Wing and Sibeck, 1997; Mühlbachler et al., 2003; Le et al., 2004], and numerical simulations [Raeder et al., 2001; Wiltberger et al., 2003]. The polar cap expands, and the polar cusp and auroral oval moves to a lower latitude associated with the magnetopause erosion as the net open flux increases [Burch, 1972; Crowley and Lockwood, 1992; Milan, 2013].

Magnetic reconnection is also the main driver for strong field-aligned currents (FACs) originating at the magnetopause boundary during southward IMF, where tangential stress exerted on magnetic field lines results in large magnetic shear (or twisting of magnetic field lines) [e.g., Hones, 1984; Cowley, 2000]. Early observations have established the association between the auroral oval and large-scale FACs [Sugiura, 1975; Kamide and Akasofu, 1976; Iijima and Potermra, 1978; Saflekos et al., 1982].

Simulations have shown that large-scale FAC sheets originating at the magnetopause boundary map to the poleward portion of the auroral oval [Tanaka, 1995]. Using observations, Xiong et al. [2014] obtained functional relationships between the latitude of auroral oval boundaries inferred from FAC intensities and confirmed that the poleward boundary of the auroral oval is closely controlled by the merging electric field on the dayside.

We report multi-mission observations of dayside solar wind-magnetosphere interaction during the main phase of the March 17, 2015 magnetic storm. While the effects of reconnection on different aspects of the system have been demonstrated previously, documenting these effects and their magnitudes simultaneously during extreme events has not previously been possible. Our multi-mission observations present evidence for all the manifestations of reconnection during storm-time conditions. The combined observations of FACs from Swarm and AMPERE, auroral emissions from DMSP, and magnetopause crossings observed by MMS and GOES provide both global and in-situ coverage of key regions of the interaction, and reveal details of magnetospheric responses for understanding the nature of the interaction.

2. Data Set Descriptions

Swarm is a three-spacecraft mission launched into a high-inclination (87.5°) low-Earth orbit on November 22, 2013 [Lühr et al., 2015]. After reaching its final constellation configuration in April 2014, Swarm-A/C fly side by side at the same altitude (~460 km) with a longitudinal separation of 1.4° and Swarm-B in a slightly higher altitude orbit (520 km). The orbit period is about 93 minutes but slightly different between A/C and B, so that their along-orbit latitudinal separation gradually changes. Their orbital planes also gradually drift apart and the separation angle increases by ~20° longitude per year. The

highly accurate magnetic field data from Swarm's Vector Field Magnetometer provide frequent in-situ measurements of FACs in the auroral zone. Meanwhile, AMPERE yields global measurements of FAC system every 10 minutes [Anderson et al., 2014] providing a continuous monitor of the global system and these data are used here to place the Swarm in-situ observations in context. AMPERE FACs are derived from global observations of magnetic field perturbations from the Iridium constellation of more than 70 near-polar orbiting satellites [Anderson et al., 2000; Waters et al., 2001].

We also use auroral emission observations from DMSP F18, which orbits Earth in a sun-synchronous polar orbit in the morning-evening sector at 850 km altitude. The Special Sensor Ultraviolet Spectral Imager (SSUSI) instrument measures auroral and airglow emissions of far ultraviolet (FUV) radiance produced by the upper atmosphere [Paxton et al., 1992a, 1992b]. SSUSI provides auroral images in five channels (1216 Å, 1304 Å, 1356 Å, LBHS and LBHL), and we use the emissions derived from the N2 LBHS channel (N_2 emissions in the 1400–1500 Å range).

GOES-13/15 as well as the newly launched MMS spacecraft provide in-situ magnetic field measurements in the magnetosphere. GOES-13/15 are two of NOAA's geosynchronous satellites located at ~75° and ~135° west geographic longitude, respectively. Singer et al. [1996] provide a description of GOES magnetometer data. The MMS mission, launched into a highly elliptical equatorial orbit on March 13, 2015 (UTC Time), contains four identical spacecraft to study magnetic reconnection [Burch et al., 2015]. The March 17, 2015 magnetic storm occurs coincidently with the magnetometer commissioning. The magnetometers were turned on to monitor the magnetometer boom deployments, all of which occurred within the main phase of the storm. A description of the MMS magnetic field investigation is provided in Russell et al. [2014] and Torbert et al. [2014].

3. Observations

On March 17, 2015, a strong magnetic storm occurred following a coronal mass ejection. Figure 1 shows the IMF and solar wind conditions from ACE as well as the SYM_H index (the 1-min high-resolution global storm index) for March 17-18. The ACE data are time-shifted by 43 minutes, determined from synchronization of the solar wind shock and the storm sudden commencement (SSC), to account for the travel time to Earth. The geomagnetic response to the SSC is a ~50 nT increase in SYM_H at ~04:48 UT. The storm main phase followed after the IMF-Bz's southward turning at ~05:59 UT. The IMF-Bz then fluctuated between north and south before it stayed strongly southward (~ -20 nT) for a prolonged period. The IMF By was predominately negative in the first 6 hours and then stayed positive. The storm main phase lasted for about 17 hours. The Dst minimum reached -223 nT.

During the storm main phase, the Swarm spacecraft made multiple crossings of the dayside auroral zone. The top panel of Figure 2 shows the orbit tracks of the Swarm spacecraft in the northern polar cap. The orbit tracks are displayed in the Magnetic Apex Coordinates [Richmond, 1995]. The three spacecraft Swarm-A/C and B are color-coded as red/blue and green, respectively. The magnetic local times in the dayside are ~7-9 for Swarm-A/C and ~8-10 for Swarm-B. There is a ~30 min lag in auroral zone crossing times between Swarm-A/C and Swarm-B. The bottom of Figure 2 shows the Swarm magnetic field observations in the morning sector indicative of FACs, with the IMF-Bz and SYM_H index repeated on the left with dashed lines (labeled from t_1 to t_{12}) to indicate the IMF and geomagnetic conditions at the times of the observations on the right. The magnetic field data are for the azimuthal component of the magnetic field residuals (δB_FAC, positive for westward deflection), which is expected to bear the largest FAC signatures. The magnitude of δB_FAC is proportional to the FAC intensity

(the linear current density in A/m per unit distance perpendicular to a presumed infinite current sheet). The magnetic field data are plotted as versus magnetic latitude to show where the currents occur. The magnetic local time at the dayside FAC crossing is noted in each panel. The AMPERE global FAC distributions are provided in Supplement 1.

Before and shortly after the SSC, when the IMF is northward, the δB_FAC perturbation is negative (eastward), corresponding to typical NBZ FACs, i.e., upward in the higher latitude edge and downward in the lower latitude edge in the morning, in an opposite sense to the region 1 (R1) and 2 (R2) FACs [Stauning, 2002]. This is confirmed by the global distribution observed by AMPERE (cf. Supplement 1). For the strongly northward IMF at time t_1 after SSC, the NBZ currents at Swarm occur in ~74°-82° MLat range with peak δB_FAC of ~500 nT. The DMSP F18 aurora image at 04:22 UT before the SSC (Figure 3a) shows typical quiet-time emissions. The next image at 06:05 UT shows enhanced aurora emissions, apparently in response to the SSC pressure pulse. The latitude range of NBZ FACs and the auroral oval in the morning side are generally in agreement.

In the next three Swarm passes at times labeled t_2 - t_4 for predominately southward IMF, it is evident that the NBZ FACs disappear and a pair of FACs develop at lower latitudes. Their magnetic field perturbations are mainly positive, corresponding to a pair of FACs flowing in the sense of morning-side R1/R2 FACs, i.e., downward (upward) at higher (lower) latitude. Their locations move in latitude, occurring most equatorward for strongest negative Bz at t_3. The Swarm observations are again confirmed by the AMPERE FAC maps (cf. Supplement 1). Two DMSP-SSUSI auroral images during this interval, 07:49 UT (Figure 3c) and 09:31 UT (Figure 3d), exhibit a very thin arc extending from noon to ~8 MLT, which is the shape typically associated

with southward IMF and is believed to be an optical signature of particle precipitation along cusp field-lines during dayside reconnection [Zhang et al., 2005]. The arc's equatorward edge, believed to be the boundary of open-closed field lines, maps to the dayside magnetopause. The IMF is southward at 07:49 UT and nearly horizontal at 09:31 UT. The lower latitude of the thin arc for the southward IMF case (Figure 3c) appears to agree with the magnetopause erosion due to dayside reconnection.

The Swarm passes for time t_5 in Figure 2 and the DMSP-SSUSI aurora image at 11:14 UT (Figure 3e) all occur during a brief interval of northward IMF. The R1/R2 FACs fade away and the NBZ FACs reappear at higher latitude as evidenced by the negative δB_FAC. The thin arc also disappears in the aurora image. The SYM_H index becomes less negative. These observations indicate that dayside reconnection ceases under northward IMF.

The IMF turns southward at ~12:00 UT and remains predominately southward for the rest of the day, which drives reconnection and fuels the continued energization of the strong storm. The evidence is the development of strong R1/R2 FACs in the Swarm (times t_6-t_{12} in Figure 2) and AMPERE observations, and the formation of the dayside thin arc in the DMSP-SSUSI auroral images (Figures 3f-3i). The FACs move equatorward from times t_6 to t_9, retract poleward following the IMF-Bz perturbation at time t_{10}, and then continue their equatorward motion at times t_{11} and t_{12}. The FACs also strengthen as they move equatorward with δB_FAC magnitudes as high as ~1500 nT when they are most equatorward. Accordingly, the dayside auroral oval expands and then contracts slightly, in agreement with the FAC observations. In particular, the auroral image at 16:19 UT (Figure 3g) is at the time when the auroral oval is most expanded to as low as ~60° MLat. This is also near the time when FACs are most equatorward with R1 FACs at ~60° Mlat (times t_8 and t_9 in Figure 2). Our observations

show that the R1 FACs and the dayside thin arc move in harmony and are generally collocated in the same latitude range, apparently in response to dayside reconnection. Because these features map to the dayside magnetopause, the expansion of the R1 FACs and auroral emissions to their most equatorward extent should correspond to the dayside magnetopause erosion.

When the auroral oval expands to as low as 60° MLat, we expect that the highly eroded magnetopause would move well inside the geosynchronous orbit. Fortuitously, GOES-13/15 geosynchronous spacecraft are positioned in the right locations during the most eroded interval to confirm this. Meanwhile, the newly launched MMS fleet, located in the pre-dawn magnetosphere, provides additional evidence for magnetopause erosion. Figure 4 shows the spacecraft orbits and magnetic field observations from GOES-13/15 and MMS-2/4. In Figure 4a, the spacecraft orbit segments for 16-17 UT are plotted in the GSE equatorial plane. This interval brackets the Swarm observations at time t_8 (Figure 2) and the DMSP-SSUSI auroral image at 16:19 UT (Figure 3g), when the FACs and auroral oval are expanded to the most equatorward latitudes. Being geosynchronous, the GOES locations at other times can be estimated in Figure 4a. Figure 4a also shows the magnetopause and bow shock under nominal conditions. These spacecraft would be positioned well inside the magnetosphere under nominal conditions. The average solar wind dynamic pressure within the 16-17 UT interval is 10.5 nPa (Figure 1). The empirical magnetopause models predict that the magnetopause standoff distance under pressure balance would be ~8 R_E [Petrinec and Russell, 1996; Shue et al, 1998]. Thus, the action of the compression by the enhanced dynamic pressure alone should not have pushed the magnetopause inside geosynchronous orbit [Rufenach et al., 1989].

Figures 4b and 4c show the magnetic field observations from GOES-13/15 and

MMS-2/4, respectively. The GOES data cover 8 hours from 12 to 20 UT with the yellow shaded interval for 16-17 UT, corresponding to locations shown in Figure 4a. The MMS data cover only 5 min (16:45:30 to 16:50:30 UT) near its brief excursion into the magnetosheath. From the GOES observations, it is evident that GOES-13 crosses the magnetopause multiple times from ~13:15 to 14:00 UT near 09 h local time, and then stays in the magnetosheath for more than three hours from 14:38 to 17:47 UT for 09-12 h local time. GOES-15, while moving from the nightside, has a few short excursions into the magnetosheath in 06-09 h local time. The MMS fleet, while still on the night side but outside the geosynchronous orbit, has one short excursion into the magnetosheath from ~16:47:00 to 16:49:20 UT. Thus, during the interval 16-17 UT, GOES-13 is in the magnetosheath near local noon, GOES-15 has a short excursion into the magnetosheath in the post-dawn sector (~16:16-16:25 UT), and MMS shows a short excursion into the magnetosheath in the pre-dawn sector (~16:47:00-16:49:20 UT).

In Figure 5, the AMPERE observations provide a global context for in-situ spacecraft measurements. The top panels are Swarm FAC density profiles at time t_8 in Figure 2 and the bottom 10-min AMPERE global FAC maps centered at the Swarm dayside FAC times, 16:08 UT for Swarm-A and 16:42 UT for Swarm-B, respectively. Swarm-A observes the dayside FACs at 16:06-16:12 UT and Swarm-B at 16:41-16:43 UT, both in agreement with the AMPERE FAC distributions. Also overlaid on the AMPERE maps are footprints of GOES-13/15 and MMS orbits for 16-17 UT. GOES-13 is near the poleward edge of the R1 FACs, GOES-15 within the R1 FACs moving towards their poleward edge, in agreement with GOES-13 being in the magnetosheath and GOES-15 mainly in the magnetospheric side with a brief excursion of the magnetosheath (Figure 4b). MMS-2/4 are in pre-dawn R1 FACs near their poleward edge. This explains why the MMS fleet, being on the nightside, also has a short excursion into the

magnetosheath (Figure 4c). Collectively, these observations provide consistent support of the existence of strong magnetopause erosion during the storm main phase.

4. Discussion and Conclusions

The observations presented in the previous section demonstrate that the magnetopause has moved inward to a location that is closer to Earth than what would have been expected based on pressure balance with the upstream solar wind. This inward displacement can be explained by the transfer of magnetic flux from the dayside magnetosphere into the magnetotail during the prolonged period of southward IMF. The erosion of the dayside magnetopause in this manner has been extensively studied [e.g., Holzer and Slavin, 1978]. Described in terms of currents, as opposed to magnetic flux transfer, erosion is caused by the enhancement of the Region 1 and tail current systems that occur during intervals of southward IMF [e.g., Maltsev and Lyatsky, 1975; Maltsev et al., 1996]. These current systems produce a southward fringe magnetic field in the dayside magnetosphere which cancels out a portion of the Earth's internal magnetic field. As a result the point where the weakened planetary magnetic field is in equilibrium with the solar wind pressure is shifted toward Earth.

The observed strong magnetopause erosion is not adequately accounted for in widely used empirical magnetopause models. The Shue et al. [1998] model, developed for extreme solar wind conditions, predicts a magnetopause with a subsolar standoff distance of 6.35 R_E and a flare parameter α of 0.729 under the average solar wind dynamic pressure (10.53 nPa) and IMF-Bz (-15.8 nT) for 16-17 UT. The subsolar standoff distance from the Shue et al., [1997] and Petrinec and Russell [1996] models are 6.44 R_E and 5.95 R_E, respectively. These models would place GOES-13 in the magnetosheath just outside the subsolar magnetopause. They keep GOES-15 and MMS

well inside the magnetopause, because the model magnetopause is too flared. In the case of the Shue et al. [1998] model, GOES-15 and MMS would be ~2 and 4 R_E inside the model magnetopause, respectively. The most likely reason for this is that during strong reconnection events, the tail lobes grow at the expense of the closed field like region, while the Shue et al. [1998] model does not account for the shape change and assumes that the noon-midnight and equatorial cross-sections are the same. The effect of strong IMF By is also not considered. Lopez et al. [2007] have demonstrated that the Lyon-Fedder-Mobarry global MHD model provides a better prediction than the empirical models during the 2003 Halloween storm. Thus, three-dimensional physics-based models driven by real solar wind parameters are the next step in understanding the interaction.

In this paper, we present multi-mission observations of FACs, auroral oval, and magnetopause crossings to understand the dayside interactions during the main phase of the March 17, 2015 magnetic storm. Dayside reconnection under southward IMF is expected to transport magnetic flux from magnetopause to tail lobes, strengthen magnetospheric currents, and lead to polar cap expansion and magnetopause erosion. Our observations assemble evidence for all these manifestations. Swarm and AMPERE observations show that dayside FACs are controlled by IMF-Bz and significantly intensified after a prolonged period of strongly southward IMF. When the IMF turns southward, the dayside auroral oval, as seen by DMSP-SSUSI, appears as a thin arc associated with ongoing dayside reconnection. Both the FACs and the auroral arc move equatorward reaching as low as ~60° MLat after a prolonged period of southward IMF. All these effects from dayside reconnection lead to strong magnetopause erosion, evident in the in-situ measurements of magnetopause crossings by GOES-13/15 and MMS. Thus, the coordinated Swarm, AMPERE, DMSP, MMS and GOES observations, with

both global and in-situ coverage of the key regions, provide a clear demonstration of the effects of dayside reconnection on the entire magnetosphere.

Acknowledgments.

We thank O. Le Contel and S. Petrinec for useful discussions. AMPERE development, data acquisition, and science processing were supported by NSF awards ATM-0739864 and ATM-1420184 to JHU/APL and all products used here are available via http://ampere.jhuapl.edu. We thank the JHU/APL SSUSI team for providing the DMSP F18 SSUSI auroral data. The European Space Agency is acknowledged for providing the Swarm data. The Swarm data used in this paper are freely accessible at https://earth.esa.int/guest/swarm/data-access. We acknowledge use of NASA/GSFC's Space Physics Data Facility's CDAWeb service for obtaining the ACE interplanetary magnetic field data, ACE solar wind plasma data, and the SYM_H index. We acknowledge use of NOAA Space Weather Prediction Center for obtaining GOES magnetometer data. We thank the entire team of NASA's MMS mission for the dedication and expertise in its successful development and operations.

References

Anderson, B. J., K. Takahashi, and A. Toth (2000), Sensing global Birkeland currents with iridium® engineering magnetometer data, Geophys. Res. Lett., 27(24), 4045-4048, DOI: 10.1029/2000GL000094.

Anderson, B. J., et al. (2014), Development of large-scale Birkeland currents determined

from the Active Magnetosphere and Planetary Electrodynamics Response Experiment, *Geophys. Res. Lett.*, *41*, DOI:10.1002/2014GL059941.

Aubry, M. P., C. T. Russell, and M. G. Kivelson (1970), Inward motion of the magnetopause before a substorm, J. Geophys. Res., 75(34), 7018–7031, doi:10.1029/JA075i034p07018.

Burch, J. L. (1972), Precipitation of low-energy electrons at high latitudes: Effects of interplanetary magnetic field and dipole tilt angle, J. Geophys. Res., 77(34), 6696–6707, doi:10.1029/JA077i034p06696.

Burch, J. L., T. E. Moore, R. B. Torbert, and B. L. Giles (2015), Magnetospheric Multiscale overview and science objectives, Space Sci. Rev., doi:10.1007/s11214-015-0164-9.

Cowley, S. W. H. and Lockwood, M. (1992), Excitation and decay of solar wind-driven flows in the magnetosphere-ionosphere system, Ann. Geophys., 10, 103–115.

Cowley, S. W. H. (2000), Magnetosphere-Ionosphere Interactions: A Tutorial Review, in Magnetospheric Current Systems (eds S.-I. Ohtani, R. Fujii, M. Hesse and R. L. Lysak), American Geophysical Union, Washington, D. C., doi: 10.1029/GM118p0091.

Dungey, J. W. (1961), Interplanetary magnetic fields and the auroral zones, *Phys. Rev. Lett.*, **6**, 47–48.

Holzer, R. E., and J. A. Slavin (1978), Magnetic flux transfer associated with expansions and contractions of the dayside magnetosphere, J. Geophys. Res., 83(A8), 3831–3839, doi:10.1029/JA083iA08p03831.

Holzer, R. E., and J. A. Slavin (1979), A correlative study of magnetic flux transfer in the magnetosphere, J. Geophys. Res., 84(A6), 2573–2578, doi:10.1029/JA084iA06p02573.

Hones, E. W. (1984), Field-Aligned Currents Near the Magnetosphere Boundary, in

Magnetospheric Currents (ed T. A. Potemra), American Geophysical Union, Washington, D. C., doi: 10.1029/GM028p0171.

Iijima, T., and T. A. Potemra (1976), Field-aligned currents in the dayside cusp observed by Triad, J. Geophys. Res., 81(34), 5971–5979, doi:10.1029/JA081i034p05971.

Iijima, T., and T. A. Potemra (1978), Large-scale characteristics of field-aligned currents associated with substorms, J. Geophys. Res., 83(A2), 599–615, doi:10.1029/JA083iA02p00599.

Kamide, Y., and S.-I. Akasofu (1976), The location of the field-aligned currents with respect to discrete auroral arcs, J. Geophys. Res., 81(22), 3999–4003, doi:10.1029/JA081i022p03999.

Le, G., Russell, C. T., and Takahashi (2004), K.: Morphology of the ring current derived from magnetic field observations, Ann. Geophys., 22, 1267-1295, doi:10.5194/angeo-22-1267-2004.

Lopez, R. E., S. Hernandez, M. Wiltberger, C.-L. Huang, E. L. Kepko, H. Spence, C. C. Goodrich, and J. G. Lyon (2007), Predicting magnetopause crossings at geosynchronous orbit during the Halloween storms, Space Weather, 5, S01005, doi:10.1029/2006SW000222.

Lühr, H., J. Park, J. W. Gjerloev, J. Rauberg, I. Michaelis, J. M. G. Merayo, and P. Brauer (2015), Field-aligned currents' scale analysis performed with the Swarm constellation, Geophys. Res. Lett., 42, 1–8, doi:10.1002/2014GL062453.

Maltsev, Y. P., and W. B. Lyatsky (1975), Field aligned currents and erosion of the dayside magnetosphere, Planet. Space Sci., 23, 1257–1260, doi:10.1016/0032-0633(75)90149-X.

Maltsev, Y. P., A. A. Arykov, E. G. Belova, B. B. Gvozdevsky, and V. V. Safargaleev (1996), Magnetic flux redistribution in the storm time magnetosphere, J. Geophys.

Res., 101(A4), 7697–7704, doi:10.1029/95JA03709.

Milan, S. E. (2013), Modeling Birkeland currents in the expanding/contracting polar cap paradigm, J. Geophys. Res. Space Physics, 118, 5532–5542, doi:10.1002/jgra.50393.

Mühlbachler, S., C. J. Farrugia, H. K. Biernat, and R. B. Torbert (2003), The geostationary field during dayside erosion events 1996–2001: A joint Wind, ACE, and GOES study, J. Geophys. Res., 108, 1418, doi:10.1029/2003JA009833, A12.

Paxton, L. J., C.-I. Meng, G. H. Fountain, B. S. Ogorzalek, E. H. Darlington, J. Goldstein, and K. Peacock (1992a), SSUSI: Horizon-to-horizon and limbviewing spectrographic imager for remote sensing of environmental parameters, Proc. SPIE, 1764, 161, doi:10.1117/12.140846.

Paxton, L. J., C. I. Meng, G. H. Fountain, B. S. Ogorzalek, E. H. Darlington, J. Goldstein, S. Geary, D. Kusnierkiewicz, S. C. Lee, and K. Peacock (1992b), Special Sensor UV Spectrographic Imager (SSUSI): An instrument description, Instrum. Planet. Terr. Atmos. Remote Sens., 1745, 2.

Petrinec, S. M., and C. T. Russell (1996), Near-Earth magnetotail shape and size as determined from the magnetopause flaring angle, J. Geophys. Res., 101(A1), 137–152, doi:10.1029/95JA02834.

Raeder, J., Y. L. Wang, T. J. Fuller- Rowell, and H. J. Singer (2001), Global simulation of space weather effects of the Bastille Day storm, Sol. Phys., 204, 323–337, doi:10.1023/A:1014228230714.

Richmond, A. D. (1995), Ionospheric electrodynamics using magnetic Apex coordinates, J. Geomag. Geoelectr., 47, 191-192, doi:10.5636/jgg.47.191.

Rufenach, C. L., R. F. Martin Jr., and H. H. Sauer (1989), A study of geosynchronous magnetopause crossings, J. Geophys. Res., 94(A11), 15125-15134, doi:10.1029/JA094iA11p15125.

Russell., C. T., et al. (2014), The Magnetospheric Multiscale Magnetometers, Space Sci. Rev., doi: 10.1007/s11214-014-0057-3.

Saflekos, N. A., R. E. Sheehan, and R. L. Carovillano (1982), Global nature of field-aligned currents and their relation to auroral phenomena, Rev. Geophys., 20(3), 709–734, doi:10.1029/RG020i003p00709.

Shue, J.-H., J. K. Chao, H. C. Fu, C. T. Russell, P. Song, K. K. Khurana, and H. J. Singer (1997), A new functional form to study the solar wind control of the magnetopause size and shape, J. Geophys. Res., 102(A5), 9497–9511, doi:10.1029/97JA00196.

Shue, J.-H., et al. (1998), Magnetopause location under extreme solar wind conditions, J. Geophys. Res., 103(A8), 17691–17700, doi:10.1029/98JA01103.

Sibeck, D. G. (1994), Signatures of flux erosion from the dayside magnetosphere, J. Geophys. Res., 99(A5), 8513–8529, doi:10.1029/93JA03298.

Sibeck, D. G., R. E. Lopez, and E. C. Roelof (1991), Solar wind control of the magnetopause shape, location, and motion, J. Geophys. Res., 96(A4), 5489–5495, doi:10.1029/90JA02464.

Singer, H.J., L. Matheson, R. Grubb, A. Newman and S.D. Bouwer (1996), Monitoring Space Weather with the GOES Magnetometers. SPIE Conference Proceedings, Vol. 2812, p. 299-308, GOES-8 and Beyond, edited by Edward R. Washwell.

Stauning, P., Field-aligned ionospheric current systems observed from Magsat and Oersted satellites during northward IMF, Geophys. Res. Lett., 29(15), doi:10.1029/2001GL013961, 2002.

Sugiura, M. (1975), Identifications of the polar cap boundary and the auroral belt in the high-altitude magnetosphere: A model for field-aligned currents, J. Geophys. Res., 80(16), 2057–2068, doi:10.1029/JA080i016p02057.

Tanaka, T. (1995), Generation mechanisms for magnetosphere-ionosphere current systems

deduced from a three-dimensional MHD simulation of the solar wind-magnetosphere-ionosphere coupling processes, J. Geophys. Res., 100(A7), 12057–12074, doi:10.1029/95JA00419.

Torbert et al. (2014), The FIELDS Instrument Suite on MMS: Scientific Objectives, Measurements, and Data Products, *Space Sci. Rev.*, DOI:10.1007/s11214-014-0109-8.

Waters, C. L., B. J. Anderson and K. Liou (2001), Estimation of global field aligned currents using Iridium magnetometer data, Geophys. Res. Lett., 28, 2165-2168, doi: 10.1029/2000GL012725.

Wiltberger, M., R. E. Lopez, and J. G. Lyon (2003), Magnetopause erosion: A global view from MHD simulation, J. Geophys. Res., 108, 1235, doi:10.1029/2002JA009564, A6.

Wing, S., and D. G. Sibeck (1997), Effects of interplanetary magnetic field z component and the solar wind dynamic pressure on the geosynchronous magnetic field, J. Geophys. Res., 102(A4), 7207–7216, doi:10.1029/97JA00150.

Xiong, C., H. Lühr, H. Wang, and M.G. Johnsen (2014), Determining the boundaries of the auroral oval from CHAMP field-aligned currents signatures – Part 1, *Ann. Geophys.*, *32*, 609–622, 2014, doi:10.5194/angeo-32-609-2014.

Zhang, Y., C.-I. Meng, L. J. Paxton, D. Morrison, B. Wolven, H. Kil, P. Newell, S. Wing, and A. B. Christensen (2005), Far-ultraviolet signature of polar cusp during southward IMF-Bz observed by TIMED/Global Ultraviolet Imager and DMSP, J. Geophys. Res., 110, A01218, doi:10.1029/2004JA010707.

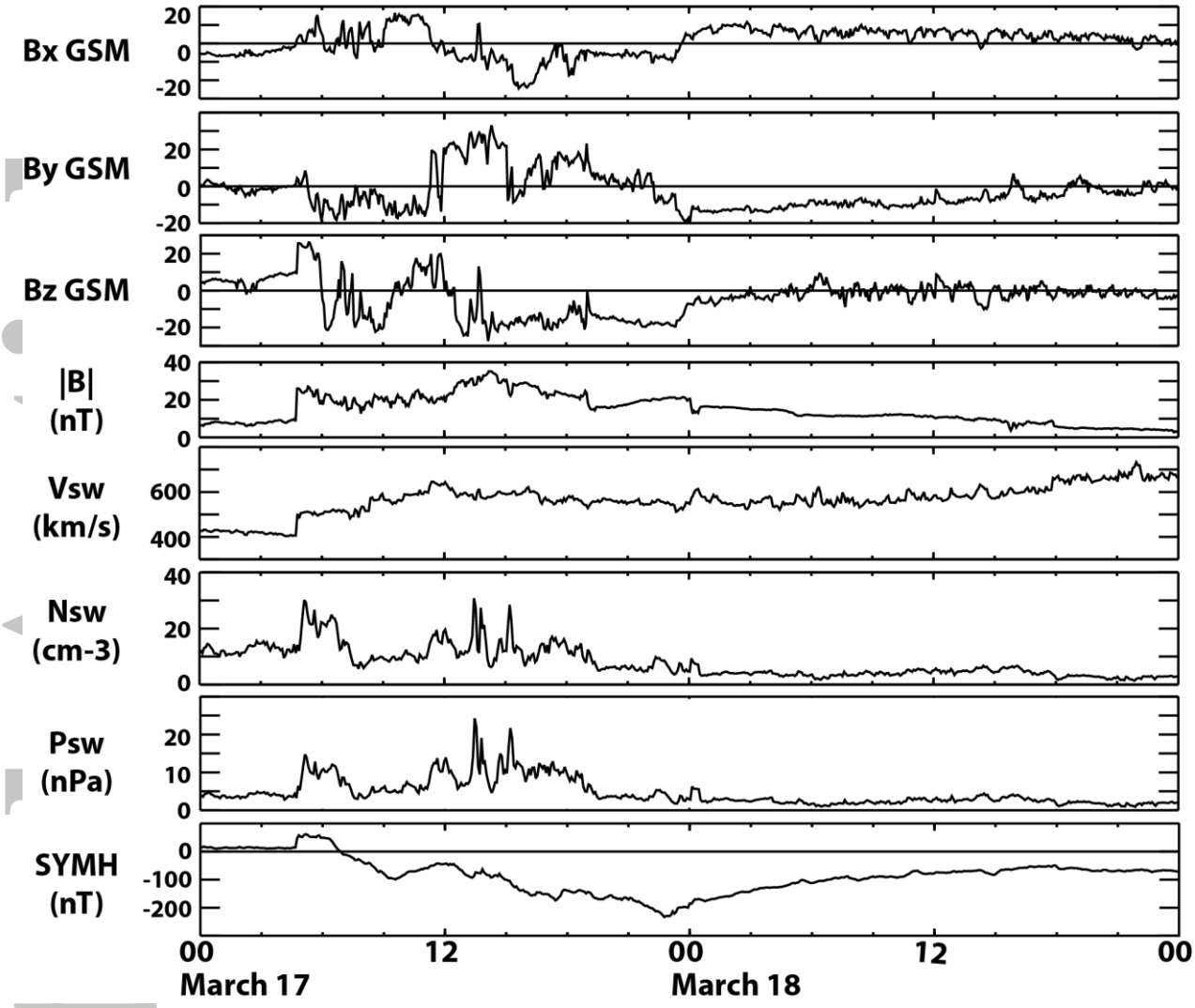

Figure 1. The IMF and solar wind data from ACE and the SYM_H index for the March 17, 2015 magnetic storm.

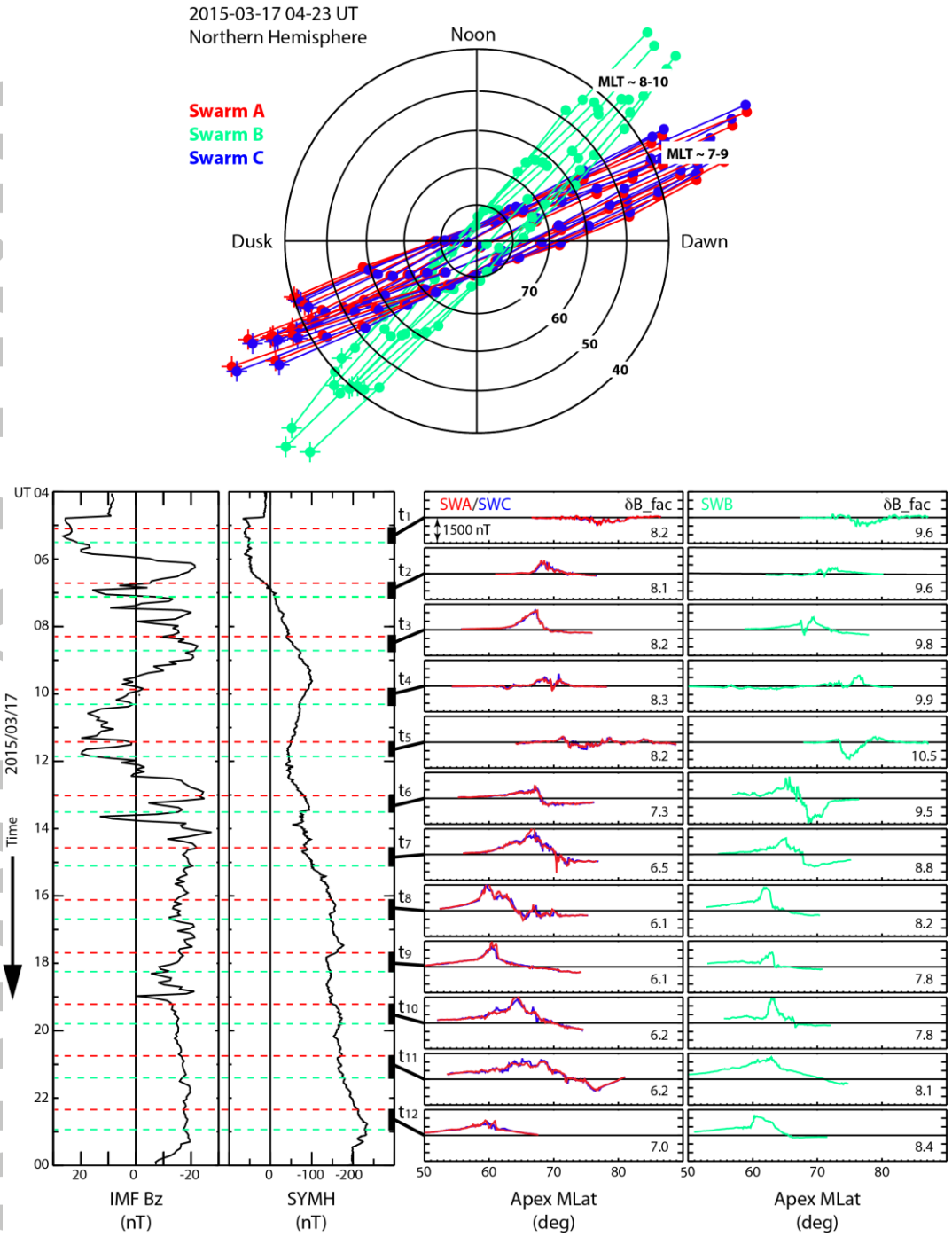

Figure 2. Swarm orbits and magnetic field observations. (Top) The Swarm orbit tracks in the northern hemisphere. (Bottom Left) time series of the IMF-Bz component and the SYM_H index. (Bottom Right) Swarm magnetic residuals δB_FAC as function of Mlat.

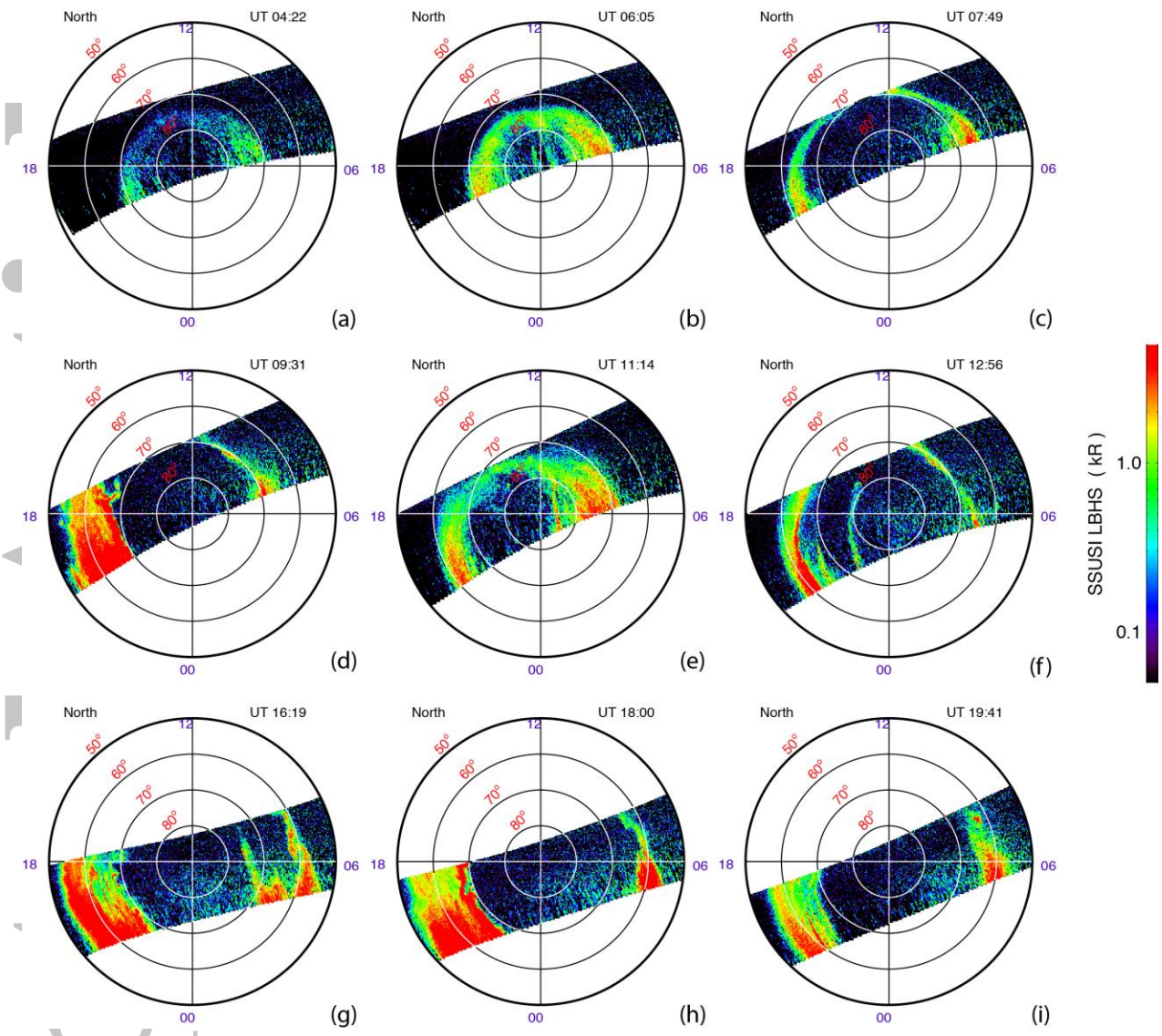

Figure 3. Auroral images from the SSUSI instrument on DMSP F18.

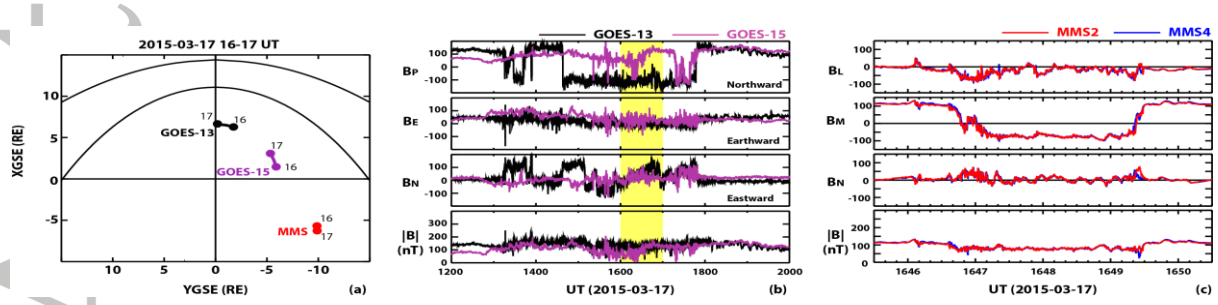

Figure 4. (a) The spacecraft orbits for 16-17 UT. (b) GOES-13/15 magnetic field data for 12-20 UT with yellow shaded interval for 16-17 UT. B_P is northward, B_E perpendicular to B_P and earthward, and B_N perpendicular to both B_P and B_E and eastward. (c) MMS-2/4 magnetic field data for 16:45:30-16:50:30 UT in the boundary normal coordination system. The magnetometer boom for MMS-2 is deployed but MMS-4 is still stowed.

.

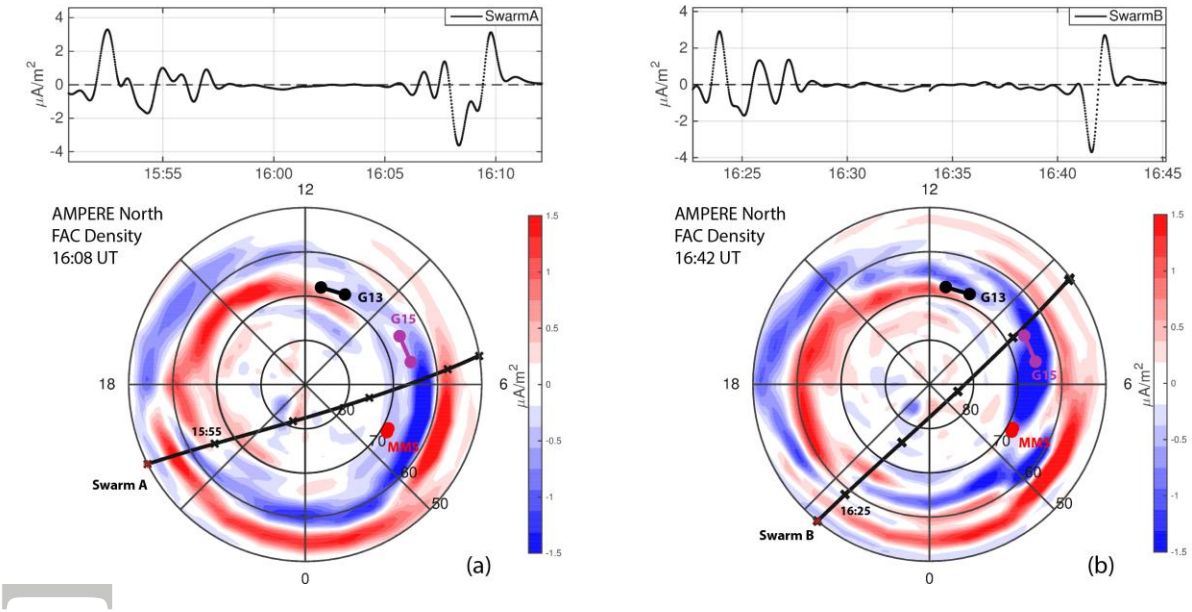

Figure 5. (Top) Swarm FAC density profiles for time t_8 in Figure 2. (Bottom) AMPERE global FAC maps derived from the magnetic field perturbations gathered over 10 min centered at the Swarm dayside FAC times. Overlaid on the AMPERE maps are spacecraft orbit tracks at their ionospheric footprints. The starting and end points of the Swarm tracks are in red and black, respectively. The tick marks within the Swarm tracks are the 5-min marks corresponding to those in the top panels. The orbit tracks for GOES-13, GOES-15 and MMS are for 16-17 UT.